Chemistry Europe
European Chemical Societies Publishing
Batteries & Supercaps

RESEARCH ARTICLE OPEN ACCESS

The Effect of Mechanical Cycling Rate, Operating Temperature, and Solvent on the Mechanics and Electronic Resistivity of Composite Electrodes

Thimo Brendel | Marcus Müller | Werner Bauer | Dominik Kramer | Reiner Mönig

Institute for Applied Materials, Karlsruhe Institute of Technology, Eggenstein-Leopoldshafen, Germany

Correspondence: Reiner Mönig (reiner.moenig@kit.edu)

Received: 2 December 2025 | **Revised:** 18 February 2026 | **Accepted:** 20 February 2026

Keywords: binder softening | lithium iron phosphate | lithium-ion battery | mechanical properties | mechanical stress

ABSTRACT

Volume changes of the active material lead to a cyclic mechanical loading of composite electrodes during operation. Active material particles and the binder mechanically interact, resulting in an evolution of the structure of the electrode. Here, we mechanically test electrodes in a cyclic compression experiment and measure their strain and resistance under conditions close to application. We investigate the effect of temperature, rate, and the presence of an electrolyte solvent on the electrode dimensions/mechanics and resistivity. We further compare the pure polymeric binder material with composite electrodes to study how the binder affects the electrode mechanics. The results demonstrate that under application conditions electrodes are even less stable and more dynamic than dry model systems. Their viscous, time-dependent mechanical behavior originates from the binder itself and is strongly affected by the presence of the electrolyte solvent, which strongly reduces the stiffness and enhances the flow of the binder. During mechanical loading and unloading, the structure of the composite evolves over the course of several cycles and adapts to the prevailing operating conditions. The properties of battery electrodes, e.g., their dimensions and their resistance, strongly depend on the state of charge, but also on their history of cycling and mechanical load.

1 | Introduction

The reliability of lithium-ion batteries has improved within recent years. Performance, durability, and longevity of lithium-ion batteries strongly depend on their chemistry, design, and operation conditions. Factors such as temperature, C-rate, and depth of discharge greatly affect the lifespan of a battery [1]. To improve lithium-ion batteries, it is essential to gain a deeper fundamental understanding of their inherent degradation processes. Many studies focus on the degradation of the active material particles [2–4], while far less is reported on the mechanics and the degradation of the passive components of electrodes [5]. This is surprising giving the importance of the mechanics for the electrical contacts in an electrode and therefore for the performance of a battery. Microscopic operando observations of electrodes are challenging but have been successfully performed [2, 6]. Here, a different approach is taken, where the electrochemical cycling is experimentally simulated by a mechanical experiment and stress, strain, and resistance are measured and used to infer mechanical processes inside the electrode. In our recent study, we electrochemically and mechanically cycled composite electrodes and identified changes in the electrode dimensions and the resistivity that develop over the course of several cycles [6, 7]. Calendered electrodes that are electrochemically cycled can expand and become increasingly porous when there is no external force acting on a cell. Similarly, a change in rate alters the structure of a conventional electrode over the course of several cycles. We explain this dynamic behavior by the reorientation and redistribution of particles inside the oscillating electrode: Individual particles move away from highly stressed regions until they reach positions in the electrode where

only moderate stresses are present during cycling [6]. This process of adaption of the electrode, i.e., the dynamic settlement of electrode particles, is unavoidable (except in the rare case of zero-strain active materials) and was observed to occur for different binder polymers to different extents. The hysteresis that was observed in the mechanical data between loading and unloading suggests that the binder of the electrode has a profound influence on the evolution of the electrode. In our previous work [6] we concentrated on mechanical experiments on dry electrodes at RT. These model systems exclude the presence of a liquid electrolyte as well as variations of the operation temperature that are relevant for real batteries. Although the previous work reveals the fundamentals of the mechanics of the composite electrode on dry model systems, it has limited use for electrodes that are immersed in an electrolyte. With the current work, we make the first steps to bridge to more realistic operating conditions of electrodes inside electrochemical cells: We address effects of the electrolyte solvent and investigate how the mechanical behavior of electrodes changes with temperature and rate. Our approach is to explore and categorize the effects of these parameters (Figure 1). This work is intended to give an overview at a fundamental and mechanistic level. Additional experiments and quantifications will be needed before the observed trends and the related knowledge can be used for the optimization of commercial batteries. Figure 1 illustrates the sequence of test conditions and the parameters that are explored in this study starting from a dry electrode at room temperature. The blue fields contain the number of the figure that contains the specified parameter.

In this experimental study, we use a purely mechanical experiment to replicate the mechanical stresses that form in the composite electrode during electrochemical cycling. This approach helps to gather information on particle rearrangement processes within the electrode coating during cell operation. The focus of this work is on the electrochemically inactive components, and in particular on the binder. The conductive additives usually form a composite structure with the binder (carbon black-binder-domain, CBD [8]). Here, individual electrode sheets are cycled mechanically to exclude electrochemical effects that additionally would alter the active material. This strategy enables the observation of the mechanics of the composite electrode, e.g., changes of the particle arrangement with cycling, and their consequences on the electronic conduction pathways through the composite. The stress levels used within this work are based on the results from operando substrate curvature measurements of the same electrodes [6], which is an established method to monitor the stress evolution in composite electrodes [9–11].

Macroscopic mechanical stresses in the composite electrode are caused by volume changes of the active material, in this case, LFP particles. As lithium ions move in and out, the particles expand and shrink. These cyclic expansions and contractions generate mechanical stresses within the composite battery electrode due to the physical connections between the active material particles, carbon black, and binder.

This study uses a mechanical compression setup, designed in-house [6], which applies compressive load to electrodes and measures their thickness and electronic resistance. With this setup, experiments can be performed reliably on individual electrode sheets or on stacks of electrodes, at different temperatures, with or without the presence of a solvent/electrolyte. Furthermore, resistance contributions from the electrode coating and the interface between coating and current collector were measured in the dry state by a commercial electrode resistance meter. Our results show that the structure of the composite electrode dynamically evolves during operation and that this depends on the applied stress rate and the prevailing conditions such as the temperature and the presence of a solvent. The binder material plays a decisive role. Here we compare electrodes with the binder polymer polyvinylidene fluoride (PVDF) and electrodes with polyacrylic acid (PAA) as the major component besides a fluorine acrylic copolymer latex (TRD).

2 | Experimental

In this work electrodes from the same batch as in [6] were used. The electrodes were prepared by dispersing LFP (SC-P2, Süd-Chemie AG) with various amounts of carbon black (CB, Super C65, Imerys) and various binder types in a dissolver mixer using N-Methyl-2-pyrrolidone (NMP) or H_2O as a solvent. NMP was applied in combination with a homopolymer PVDF binder (Kynar HSV900, Arkema), while H_2O was applied for PAA (1.25M g/mol)/TRD (TRD202A, JSR Micro). Detailed data of the LFP active material are shown in Table S1 in the Supporting Information. After homogenization, the cathode slurries were coated onto aluminum foil (20 µm thickness) using a laboratory coater with in-line drying (KTF-S, Mathis). The compositions of the different electrodes with their names are listed in Table 1. SEM images of the electrodes can be found in a previous publication [6]. For reference, a PVDF homopolymer foil with a thickness of ~500 µm (RCT Reichelt Chemietechnik) was tested as received. Propylene carbonate (PC) from Sigma-Aldrich was used as a solvent and was added to the composite electrodes or the PVDF foil in some of the experiments.

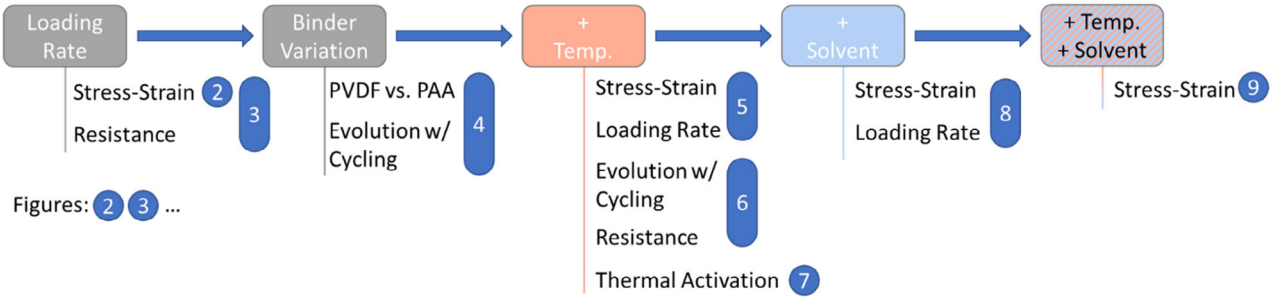

FIGURE 1 | Sequence of test conditions (horizontal row) and parameters (vertical rows) covered in this study. The grey boxes indicate an electrode in the dry state at room temperature.

TABLE 1 | Composition of the $LiFePO_4$-based electrodes and the thickness of the coatings. The electrodes are named after their majority binder component. All coatings are attached to an aluminum current collector of 20 µm thickness.

Name of electrode		LFP 5 wt% PVDF	LFP 10 wt% PVDF	LFP PAA
Weight percent [%]	LFP	85	85	87.0
	CB	10	5	8.7
	PVDF	5	10	0
	TRD	0	0	1.7
	PAA	0	0	2.6
Thickness [µm]		90	80	44
Porosity [%]		64.6	63.9	58.1
Mass loading [mg/cm^2]		10	10	5.2

The samples were investigated using the mechanical compression setup introduced in [6], here it was additionally adapted for measurements at elevated temperatures and the presence of a solvent. A photo of the setup is shown in Figure S7. The setup has a testing area of 113.1 mm^2 and can apply stresses between 50 kPa and 1.45 MPa [6]. Lateral flow of the electrode and edge effects can be neglected with this setup. First, the edges of the electrodes are not mechanically loaded because the electrode sheets were larger than the lower plate of the compression setup that defines the area under load. Second, the thicknesses of the electrodes are about two orders of magnitude below the width of the plate and the electrodes were mostly tested when they were still attached to their current collector (Figure 2a,b). Here the aspect ratio and the adhesion are both expected to strongly suppress lateral flow. In contrast to the electrodes, PVDF sheets do not cover the full test area, due to a smaller sample size, but the same forces were applied. This leads to significantly higher stresses of up to 17 MPa in the case of PVDF. During electrode operation of a cell, stresses of this magnitude are expected to act on the binder bridges at the contact points between the active material particles due to stress concentrations. During the operation of an electrode inside a cell, the active material expands and shrinks. For example, by concentration gradients or phase transformations inside the particles, large stresses reaching the GPa range can develop. These stresses are not present at the level of the composite electrode where the active particles are embedded in the compliant porous electrode and connected by the polymeric binder. Stresses in our electrodes therefore are of the order of 1 MPa or below (Figure S1 in [6]). The stresses that we apply here are of similar level or slightly higher. We use uniaxial compression which is different from the more isotropic loading during operation but since in both cases, the forces are deflected many times in the electrode structure, the stress states may share similarity. Testing electrodes purely mechanically excludes electrochemical effects in the active material and enables investigations of the reliability of the composite electrode (binder and conductive additive) at higher speed than in electrochemical cells.

The thickness of the sample (electrode/PVDF foil) was measured by three high-resolution capacitive sensors in a triangle arrangement. This configuration enables a reliable measurement of the total thickness as well as the detection of tilting of the top plate caused by a nonuniform compression of the samples. The evolution of the electrode conductivity was recorded by a four-point resistance measurement between the bottom plate and the top plate. In the case of deliberately detached coatings, the resistance was measured between two contacts attached to it. The different configurations are depicted in Figure 2. Besides the compression setup, the resistivity of the composite electrodes was measured using a commercial electrode resistance meter (Hioki RM2610). This is used directly on the electrode coatings and does not require special surface treatments or an insulating substrate. The device fits the measurements to a finite volume model and calculates the volumetric resistivity of the coating as well as the resistivity of the interface between coating and current collector. Based on this local resistivity data of volume and interface, an electrical resistance between the electrode surface and the current collector can be calculated. Further information can be found in the instruction manual provided by the manufacturer [12]. In the compression setup, the resistance between the surface and the current collector is recorded during our experiments. Since the dimensions of the tested electrode samples are known (height and area), the resistance values can be compared between both measurement techniques.

Measurements in the compression setup were performed using different sample configurations as schematically depicted in Figure 2:

(a) uses a single electrode with its coating facing downwards (in contact with the circular sample pad). This arrangement aims at the measurement of the mechanics of single

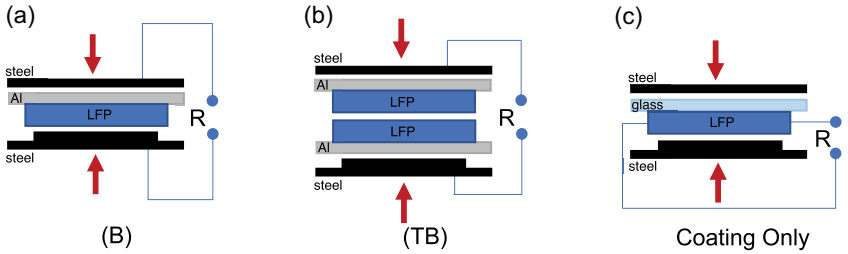

FIGURE 2 | Different measurement configurations of the compression setup, using one (a) or two (b) electrode samples. The naming scheme is related to the orientation of the coating during the experiments, namely at the bottom (B) or the top (T) of the current collector. The electrode coating without a current collector (c) uses a glass substrate for mechanical stabilization. In configuration (c), the resistance is measured in-plane. All samples are tested under compressive stress (red arrows).

electrode sheets. The interface between the coating and the steel plate of the compression setup adds a significant resistance to the electronic pathway, which limits the validity of the quantitative resistance results.

(b) uses a stack of two electrodes with their coatings in the middle and their current collectors facing towards the plates. This provides a good electronic contact between the setup and the samples, but only the combined mechanical properties of the stack can be determined. Stacks of more than two electrodes were used to amplify the mechanical signal, where needed.

(c) uses a coating that was separated from the current collector. This arrangement is targeted at the determination of the stress-resistance characteristic of the electrode coating itself excluding the impact of the interface to the current collector. The coating of an electrode with high binder content (LFP 10 wt% PVDF) was detached from the aluminum current collector by soaking it in PC and heating it on a hot plate at around 100°C for 2–3 min. This significantly intensified and accelerated the swelling (solvent uptake) of the PVDF binder [13]. Ultimately, the coating detached from the current collector and was then transferred onto a glass slide for drying. Subsequently, the resistivity of the dried composite coating is measured between two tin tabs which have been glued onto the electrode layer by a silver glue (Plano GmbH, ACHESON 1415), see Figure S2. The resistances of the glue and the tin tabs (∼40 mΩ) do not significantly contribute to the measured resistance (>5 kΩ), i.e., the resistance value measured at the tin tabs can be assumed to originate from the coating only. All parts of the electrode that are not in direct contact with the compression setup were covered by polyimide films for electrical isolation and to improve mechanical stability during handling.

To mimic the conditions during battery operation and to reveal the impact of rate on the change of morphology, stress rates between 2.5 and 8500 kPa/s (time for a full cycle from 1200 to 0.33 s) were used. For the determination of the thermal activation energy, stress jumps were applied and the time-dependent deformation was measured (stress control). Besides the stress, the prevailing conditions were varied. Experiments were performed between 22°C and 69°C, and with or without the presence of a solvent, which is used to mimic the effect of the electrolyte during electrochemical operation. PC was used as a representative for an electrolyte system. This is a strong simplification compared to typical electrolytes, but PC was needed because of its low vapor pressure to avoid evaporation during the experiments. Electrolyte salts were omitted because the tests were performed in atmosphere and decomposition reactions needed to be avoided. This may be justified since salts are not expected to strongly interfere with the electrode structure and alter the properties of the nonpolar PVDF polymer.

Changes in the mechanical properties of composite electrodes and pure binder due to a temperature change are evaluated by the calculation of their activation energies. Here, only little emphasis is given to the development of a physically correct description of the complex thermally activated deformation behavior of PVDF, instead we use a conceptually simple model to compare the deformation of bulk PVDF foil with the deformation of a composite electrode. The measured deformation behavior was fitted to a Zener_k model for both cases. A schematic of this model is given in Figure 8 and Equation (2.1) describes it.

$$\boldsymbol{\varepsilon}(\boldsymbol{t}) = \frac{\boldsymbol{\sigma_0}}{\boldsymbol{E2}} + \frac{\boldsymbol{\sigma_0}}{\boldsymbol{E1}}\left(\mathbf{1} - \exp\left(-\frac{(\boldsymbol{t}-\boldsymbol{t_0})}{\boldsymbol{\eta}/\boldsymbol{E1}}\right)\right) \tag{2.1}$$

with the Young's moduli $E1$ and $E2$, the linear viscosity $\boldsymbol{\eta}$, the external stress σ_0, and the strain $\varepsilon(t)$. The experimental data was fitted separately for two regions:

(1) at the moment of instantaneous compression: The thickness before ($t < 0$ s) and after applying the load (at $t = 1$ s) is compared to determine the strain and calculate $E2$.

(2) between 30 and 300 s after the application of the load. This period of time is chosen to account for the limitations of the simple Zener model and that a fit of the entire curve in reality requires multiple viscoelastic elements. The lower boundary excludes the region of fast straining within the first few seconds after the stress application. The higher boundary reduces the contribution of long-term creep, which becomes more pronounced at rising temperatures and with extended time of the stress application.

The fits to the raw data can be found in Figure S3 and Table S4.

Based on the measurement data, the values for the elastic moduli E and the viscosity η are calculated. Deformation is assumed to be a thermally activated process and follows an Arrhenius law with activation energies $E_{A,E1}$, $E_{A,E2}$, and $E_{A,\eta}$ given in kJ/mol

$$E(\boldsymbol{T}) = E_{\mathbf{0}} \cdot \exp\left(-\frac{\boldsymbol{E}_{\mathbf{A},E}}{\boldsymbol{R}\cdot\boldsymbol{T}}\right) \tag{2.2}$$

$$\boldsymbol{\eta}(\boldsymbol{T}) = \boldsymbol{\eta_0} \cdot \exp\left(-\frac{\boldsymbol{E}_{\mathbf{A},\eta}}{\boldsymbol{R}\cdot\boldsymbol{T}}\right) \tag{2.3}$$

Here absolute temperature T [K], the universal gas constant R [J/mol K], and the activation energy E_A (kJ/mol) per mol are used.

3 | Results

The following sections contain experimental data and observations of aspects that control the electrical and mechanical behavior of electrodes. An interpretation and discussion of this data will be given in a separate discussion later.

3.1 | Rate-Dependent Deformation of Dry Electrodes at RT

Our experiments show that the mechanical deformation of electrodes depends on rate. In Figure 3 we compare the changes in electrode thickness and resistance due to the application of compressive stresses with different rates. The rates correspond to times for full cycles of 30 (100 kPa/s), 120 (25 kPa/s), and 1200 s (2.5 kPa/s). A stack of two electrodes was used in a (TB) arrangement, as shown in Figure 2. Low rates yield slightly higher strains and resistance amplitudes. The maximum strain of the electrode differs between the highest and the lowest rate by 11%. The resistance change within a full cycle is about 5% higher at the lowest rate.

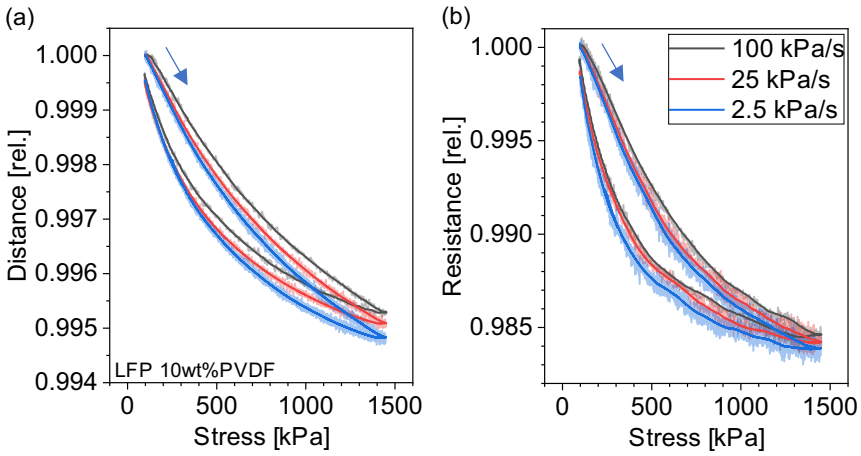

FIGURE 3 | Relative change of thickness (a) and resistance (b) of LFP-based composite electrodes on aluminum current collectors generated by compressive stress oscillations with a triangle profile at rates of 2.5, 25, and 100 kPa/s. A stack of two electrodes in (TB) configuration was used and the resistance was measured perpendicular to the electrode layer. The data for each rate shows the average of 10 cycles (data in the lighter color in the background). Solid lines were obtained by smoothing (moving average) the averaged data to help to distinguish between the curves.

The mechanical and electrical behavior of the electrode can be separated between the bulk and the interfaces. The bulk consists of the porous coating while the interface is considered to be two-dimensional and is related to the electrical contact between the coating and the current collector. The contributions of interface and bulk to the resistance were determined by a commercial resistance meter (HIOKI RM2610). For an LFP electrode (10 wt% PVDF), an interface resistivity of (17.1 ± 1.5) Ωcm^2 and a bulk resistivity of (13.7 ± 0.5) Ωcm was measured. For the sample size of the electrode used in our compression setup, this translates to a resistance of the interface of 15.12 Ω (99.3%) and of the bulk of only 0.10 Ω (0.7%). The contribution of the aluminum current collector to the resistance can be neglected.

The use of electrode layers that are detached from their current collector allows for an isolated investigation of the rate dependence of the electrode bulk without the effects of the interface to the current collector. The electrode configuration during the measurement is depicted on the right side of Figure 2. Figure 4 shows the stress-resistances measurements for the same loading rates as used in Figure 3. For the pure electrode coating without a current collector, a qualitatively similar dependence of resistance on stress is found.

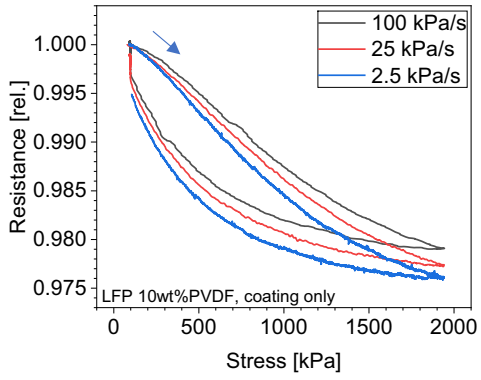

FIGURE 4 | Relative resistance changes for different stress rates of an LFP-based composite electrode (detached from its current collector). Here, the resistance was measured in the plane of the electrode.

During cycling, the stress rate does not only impact the strain and resistance amplitude within a single cycle, but leads to a long-term evolution of the electrode over many cycles. Figure 5 compares the evolution of the sample thickness for cycling rates between 5 and 8500 kPa/s. The experiments were performed up to different numbers of cycles between $5{\cdot}10^2$ and $1{\cdot}10^6$. Electrodes with the same active material and the different binder materials PVDF (a) and PAA (b) are used. In the experiments, individual electrode sheets were tested according to Figure 2b. For electrodes with PVDF binder, lower rates lead to increased densification of the electrode. This happens within shorter times and fewer cycles than for higher rates. For electrodes with PAA binder, there is no significant difference in the dynamic densification versus time.

3.2 | Deformation at Elevated Temperatures and the Effect of a Solvent

The cyclic compression of electrodes at two different temperatures is shown in Figure 6. Here, the stress–strain characteristic of an electrode that was extensively cycled at 23°C (reference) is

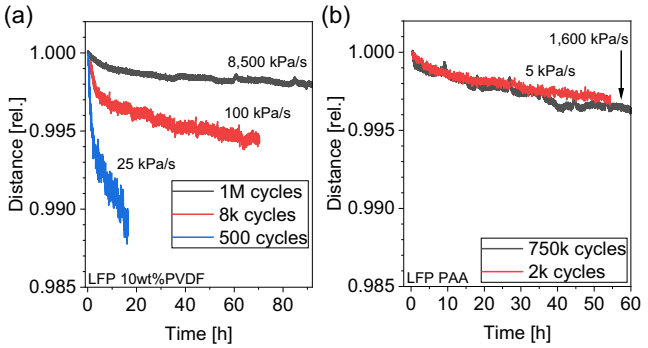

FIGURE 5 | Evolution of the sample thickness at different stress rates during extended mechanical cycling. (a) LPF-based sample (b) with 10 wt% PVDF binder at 25, 100, and 8500 kPa/s. (b) LPF-based sample (B) with PAA binder at 5 and 1600 kPa/s. The distance is reported relative to the initial thickness of the individual composite coatings.

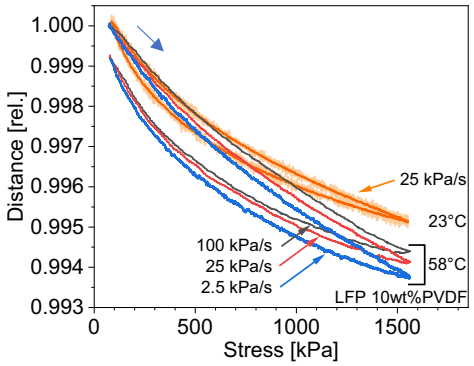

FIGURE 6 | The effect of rate at elevated temperature: Compression behavior of an LFP-based sample with 10 wt% PVDF at 23°C (reference) and 58°C, and its dependence on the stress rate at high temperature. A stack of four electrodes in (TTBB) configuration was used.

compared to its behavior at different stress rates (2.5, 25, and 100 kPa/s) directly after a temperature increase to 58°C. As a consequence, compression amplitude, hysteresis, and rate-dependency increase. In the experiment, a stack of four electrodes ((TTBB) arrangement, LFP 10 wt% PVDF coatings) was used to improve the signal-to-noise ratio. The curves are smoothed by a moving average filter (50 datapoints). The raw data with their scatter are exemplarily shown in the background of the reference curve.

During extended mechanical cycling, the composite electrode shows a settling process, which is apparent in a reduction of sample thickness, as well as in the amplitudes of thickness and resistance. At RT, this evolution was already introduced in a previous publication [6]. A change in temperature leads to a significant change in the mechanical behavior under load. Figure 7a depicts three sections at 22°C, 40°C, and 60°C, each containing 100 cycles. The evolution of the sample thickness and the resistance is shown for three individual cycles for each temperature (cycles 1, 20, and 99 in each section) in Figure 7b,c. The experiment uses a single electrode sample with an LFP 5 wt% PVDF coating. After each temperature increase, the electrode sample reaches higher values of total compressive strain, compression amplitude, and resistance amplitude, followed by a settling process during the subsequent cycling at constant temperature. Once 100 cycles were reached the load was reduced close to zero. This relaxation leads to and an increase in the thickness versus time before the temperature was raised.

The impact of the temperature on the mechanical properties of the pure PVDF binder material and a composite electrode with 5 wt% PVDF was investigated in a temperature range between 23°C and 69°C. The sample was loaded by a load jump to a constant stress and its compressive strain was recorded versus time. In the case of the composite electrode, four single sheets were stacked (TBTB) to increase the recorded signal and to equalize possible differences. From the strain evolution over time (Figure S3), the elastic moduli E2 and E1 as well as the viscosity η were obtained using the Zener$_k$ model. The fit parameters are shown in the form of Arrhenius plots in Figure 8 according to Equation (2.2) and (2.3). Table 2 lists the resulting (apparent) activation energies for both pure PVDF and the LFP electrode with PVDF binder. We use the term "apparent" because we rely on a conceptually simple Zener$_k$ model for the polymer and for the porous composite material. In particular in the latter case,

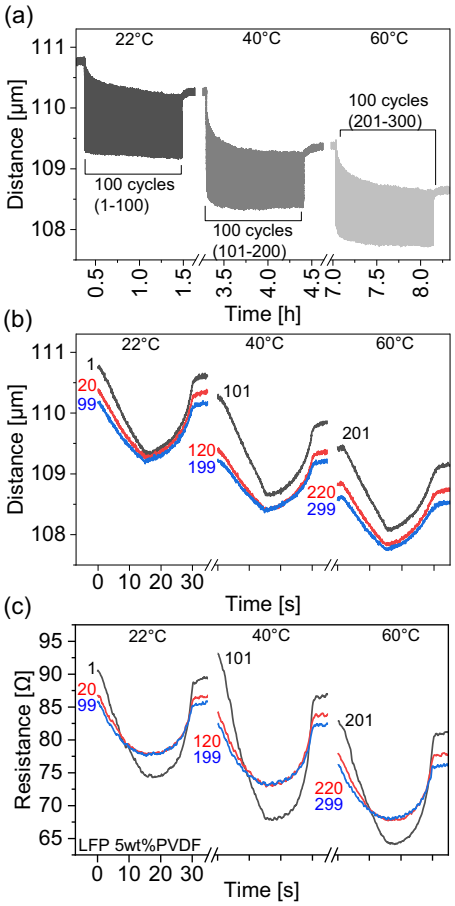

FIGURE 7 | Evolution of (a,b) sample thickness and (c) resistance for cycling at 22°C, 40°C, and 60°C for LFP samples with 5 wt% PVDF, measured in configuration (B). Here, distance is the combined thickness of coating and current collector.

this description may be of limited validity, but nevertheless is used to be able to compare the mechanical response of both materials. Figure 8 shows that for all temperatures both moduli and the viscosity are reduced for the composite electrode. The activation energies for the elastic modulus E2 are very similar in both samples and the activation energy of E1 and η are about three times higher for bulk PVDF.

In real cells, the electrodes are soaked with the electrolyte. In order to investigate electrodes that are closer to battery application, the electrodes are soaked with PC. The presence of the solvent considerably changes the mechanical properties of the electrode. The PVDF binder takes up the solvent and swells [13], which strongly changes the stress state of the coating. Figure 9 depicts stress rate tests on the same electrode sample before and after the addition of PC. The cycles are taken from a consecutive series of cycles at constant rate, i.e., the samples may not be fully relaxed at the beginning of the stress application. The solvent soaked electrode shows significantly higher strain amplitudes (up to factor 7) and a stronger influence of the rate. For dry electrodes, the amplitude of the oscillation of sample thickness varies by roughly 10% between the different rates and for the soaked ones it varies by ~ 70%. Electrodes with PAA only show minor changes of their compression behavior when soaked with PC (see Figure S6). For this reason, electrodes with PAA binder will not be covered in detail here.

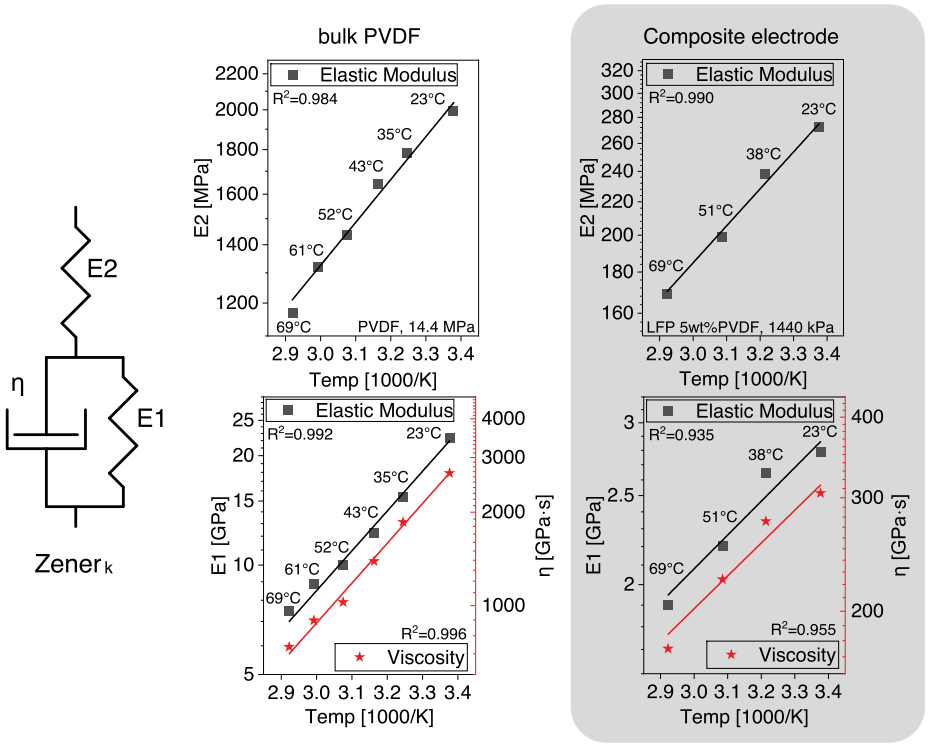

FIGURE 8 | Arrhenius plots of E2, E1, and η for pure PVDF binder (left column) and the LFP 5 wt% PVDF electrode (right column). Data points were obtained using the Zener$_k$ model. Solid lines are the fits by the Arrhenius equation.

TABLE 2 | Results of the fit of the activation energies of the mechanical properties elasticity (E2, E1) and viscosity (η) for the LFP 5 wt% PVDF electrode and for pure PVDF polymer. The listed activation energies are an apparent temperature sensitivity of the effective model parameters. The model used is strongly simplified regarding underlying physical and chemical mechanism and the energies should not be considered as unique molecular/atomic barriers.

Activation energy of	bulk PVDF	LFP 5 wt% PVDF
Elastic modulus E2	9.46 kJ/mol (0.098 eV)	8.78 kJ/mol (0.091 eV)
Elastic modulus E1	20.9 kJ/mol (0.217 eV)	7.04 kJ/mol (0.073 eV)
Viscosity η	24.6 kJ/mol (0.255 eV)	9.74 kJ/mol (0.101 eV)

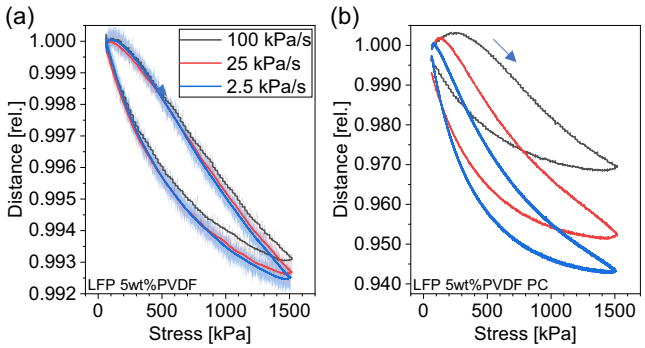

FIGURE 9 | Compressive oscillation of a single LFP electrode with 5 wt% PVDF at different stress rates in the dry state (a) and with PC solvent (b).

Figure 10a depicts a dry and a solvent soaked pure PVDF sample after a jump to a constant stress level. Here, a higher instantaneous compression (factor of ~2) and a more pronounced time-dependent compression is observed in the wet sample. Figure 10b shows the behavior during mechanical cycling at temperatures of 23°C and 52°C in the dry state, as well as at 23°C, 43°C, and 51°C in the PC soaked state. The stress–strain behavior of pure PVDF in Figure 10b shows similarities to the behavior of the composite electrode in dry (Figure 9a) and wet (Figure 9b) state. The increases in temperature as well as the application of the solvent leads to a higher compressibility and much stronger viscoelastic effects (hysteresis). Data of the impact of the liquid on the rate dependence can be found in the Figure S5.

4 | Discussion

4.1 | The Behavior of Composite Electrodes in the Bulk and at Their Interface, Rate Dependence, and the Effect of Different Binder Polymers

Mechanical cycling of a composite electrode yields different strain and resistance amplitudes depending on the applied stress rate (Figure 3). The general trends in the curves correspond to the ones previously published [6]. Deviations from these trends arise due to the differences in rate. The displacement amplitude is 11% higher at the lowest rate (2.5 kPa/s) compared to the highest rate (100 kPa/s). The associated resistance amplitude, as measured through the thickness of the electrode, is higher at the lowest rate by about 5%. Although relatively small, these trends show that the structural adaption processes in the composite electrode are time-dependent.

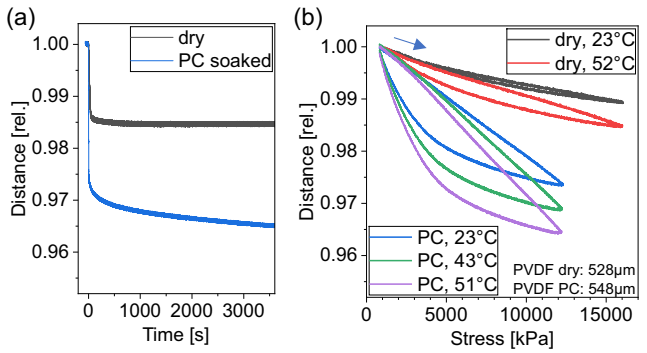

FIGURE 10 | (a) Time-dependent deformation of pure PVDF in dry and PC soaked state after stress jumps of about 15.0 (dry) and 12.3 MPa (soaked). (b) Stress–strain behavior in the dry and the solvent soaked state at different temperatures. The time for a full cycle was 120 s. The maximum stresses in the soaked sample were about 20% lower because of limited applicable force of the actuator and differences in sample size.

The mechanical response, i.e., the oscillation of the thickness of the electrode during mechanical cycling, is mostly defined by the properties of the electrode coating, as no significant compression or deformation of the metallic current collector occurs at the applied stress levels. The electrode resistance depends on the contributions from both the electrode coating and from its interface with the aluminum current collector. Here, the resistivity measurements (HIOKI RM2610) reveal that for the LFP based electrodes, the interface accounts for ∼99% and the coating only for ∼1% of the total through-thickness resistance. Aluminum with its high electrical conductivity does not contribute to the high interface resistance. The comparison of measurements on electrodes with (resistance through the electrode) and detached electrodes (resistance along the electrode) show the strong influence of the current collector interface on the electrode resistance. The shapes of the curves in Figure 3b are qualitatively similar to the ones in Figure 4 where the resistance of an electrode without a current collector was measured along its length. This suggests that similar mechanisms are present in the contact mechanics between individual particles inside the bulk of the electrode and between particles and the planar current collector at the interface. When comparing the contact mechanics of two vertically aligned particles in the bulk (mirror symmetry of the deformation of both spherical particles) with that of a single particle on top of the flat current collector, it becomes apparent that the configurations may be mechanically and electrically similar. The existing minor differences between Figures 3b and 4 may be explained by alterations of the electrode that happen during its detachment from the current collector. The detachment was performed with the help of a solvent and subsequent drying. This may increase porosity and allow for greater particle rearrangements and therefore may contribute to the observed larger rate sensitivity. The observed strong contribution of the interface to the through electrode resistance may be explained by a native oxide that always covers the aluminum current collector.

The stress rate impacts the settling process of the electrode during extended cycling. Figure 5 depicts the thickness reduction during the mechanical cycling of LFP-based electrodes with 10 wt% PVDF and PAA binder over a range of rates within a factor of 340. For the PVDF binder, the compaction is slower when higher rates are applied. In contrast to PVDF, the compaction of the electrode with PAA does not seem to depend on the applied rate. It appears to depend only on the time of load application, i.e., similar levels of compression are obtained after the same time for the low and the high rate. Probably this is linked to the different mechanical properties of PAA and PVDF. At RT, PAA is well below its glass transition temperature (∼130°C) and therefore mostly deforms elastically with very little viscoelastic or plastic deformation [14, 15]. On the contrary, PVDF is well above its glass transition temperature (about −40°C) and therefore is more viscous [16]. The elastomeric TRD contained in the PAA electrodes clearly does not play a decisive role in their mechanical properties. The results indicate that these are dominated by the stiffer PAA. For the reason of simplification, only PAA will be referred to as the binder in the further course of this work.

4.2 | The Impact of the Temperature on the Evolution of the Electrode

Figure 6 shows the consequences of a temperature change from 23°C to 58°C for a composite electrode with 10 wt% PVDF. The orange reference curve was measured at RT and the red curve was recorded at the same rate after a temperature change to 58°C. Besides a higher compressibility, a significant increase in the hysteresis is found at higher temperature. Both observations agree with the data on pure PVDF binder measured at different temperatures (Figure S5a/b). In polymers, an increase in compressibility can be reached either by raising the temperature or by lowering the stress rate (in our electrode this corresponds to going through the curves from black to red to blue in the measured data in the figures). The effect of rate and temperature was discussed in detail for several amorphous polymers by Mulliken and Boyce [17].

Temperature changes not only trigger immediate responses, they also change the evolution of thickness and resistivity during continued cycling. Figure 7 resembles the operation of a cell at different temperatures and illustrates the effects of changes in temperature: Every temperature step leads to a decrease in the thickness of the electrode. This means that the particles in the electrode rearrange directly after the temperature change. From calendering, it is known that the reduction in the adhesive strength of the binder at higher temperatures leads to denser electrodes where the lower adhesive force allows for the additional movement of the particles in the electrode [18, 19]. Based on these findings we also attribute the observed densification of the electrode in Figure 7a to the temperature dependent adhesive force of the binder and suggest that this phenomenon is important for cells that operate under changing temperatures. It should be noted that the increased temperature not only reduces the adhesive force but affects the mechanical properties of the binder in general. For example, the decreased viscosity and the reduced yield strength are also expected [17] to contribute to the more pronounced changes of the electrodes that we observe at higher temperatures. Each temperature change appears to trigger a new settling process, characterized by the reduction of the compression and resistance amplitude versus time. We use the term settling to describe the redistribution of particles within the electrode caused by cyclic mechanical forces [6]. Although we do not have a visual proof of the rearrangement of particles, the combination of our strain and resistance data strongly suggest that this process happens. The rearrangements are expected

to be highly dynamic during electrochemical or mechanical cycling where they build up and partially relax. They accumulate over several cycles to cause the described settling that can explain the evolution in Figure 7. The rearrangement of particles and binders after several cycles has been observed in the literature for example by AFM [20] and X-ray based tomography [21].

In Figure 7, after 100 cycles at RT, the temperature was raised to 40°C and the compression amplitude in cycle 101 increases by 25% (from 0.89 to 1.13 μm) in Figure 7b. During the subsequent cycling at 40°C, the electrode settles again and the thickness amplitude reduces to 69 % of the amplitude of cycle 101 in cycle 200. The settling is slightly faster compared to the settling at 22°C. A similar behavior is observed for the second temperature step, with an increase in amplitude of approximately 29% (from 0.78 to 1.01 μm) in cycle 201. The increased compression amplitudes directly after the temperature changes are in good agreement with the change of the elastic moduli that we measured by the compression experiments of pure PVDF polymer at different temperatures (values for E2 in Figure 8). Based on the fit data, the anticipated strain increase is ∼25 % for both temperature changes from 22°C to 40°C and from 40°C to 60°C. Therefore, it is reasonable to assume that the instant increase in compressibility of the composite electrode upon changing the temperature is mostly due to the property change of the PVDF binder. We assume that the viscous properties of the binder contribute to the settling that takes place during the subsequent continuous cycling at constant temperature. In the composite electrode, the movement of the binder also impacts the conductive pathways, as the positions of the carbon black particles commonly change together with the binder. This can be seen by the trend towards lower resistances with rising temperatures (see Figure 7c), which resembles the compaction of the electrode (Figure 7b).

4.3 | The Role of the Binder in the Mechanics of the Composite Electrode

Electrodes are composed of metals, ceramics, and polymers. Among these classes of materials only polymers show a strong dependence of their mechanical properties on temperature. The pronounced thermal effects described in the previous section indicate that the binder polymer influences the mechanical behavior of the composite electrode. Figure 8 gives further insights into the temperature dependence of the mechanical properties of both, pure PVDF polymer and a typical PVDF-based electrode. Here we report on measurements of stress jumps (Figure S3). Besides elasticity, most binder materials show a nonlinear time-dependent deformation (e.g., viscous behavior). The detailed behavior depends on the molecular structure of the polymer and can be complex so that a correct description of the stress–strain evolution requires several time constants. Here we rely on a Zener_k model to describe the deformation and extract (apparent) thermal activation energies. Here we want to compare two mechanically very different materials that are expected to show thermal activation and therefore we refrain from very detailed models and instead use this conceptually simple model. The fit results are shown in Figure 8 and in Table 2. The fits of the stress jump data yield the elastic modulus E2 that is responsible for the time-independent deformation, i.e., instantaneous strain upon the stress jump, as well as the elastic modulus E1 and the viscosity η, which together describe the evolution of the strain versus time after the jump (Equation (2.1)). The modulus E2 describes the nontime-dependent elastic deformation. According to Figure 8, it is reduced by almost one order of magnitude in the composite electrode which may be attributed to its porosity, i.e., reduced relative density [22]. The activation energy is in good agreement with that of bulk PVDF. Therefore, it seems plausible that the polymer accounts for a large part of the elastic behavior of the electrode. Active material and carbon black are expected to show athermal mechanical behavior. The fact that E1 and η are thermally activated indicates the effect of the polymer. Again, the modulus and viscosity are significantly smaller in the composite which may be explained by the porosity and the corresponding smaller relative density. For the time-dependent deformation path (E1 and η) the thermal activation is roughly three times lower than for the bulk polymer. This may be related to a mechanistic difference in the deformation pathways of the bulk polymer and the binder bridges in the composite.

We suggest an alternative explanation that relates to the time dependence and the particular deformation path of electrodes. At short times after a load step, the binder joints dominate the stress–strain behavior of the composite with a behavior similar to bulk PVDF. With ongoing time under load, particles and binder move by viscous and plastic flow in a way that the binder is increasingly depleted in highly stressed regions and more and more direct contacts among the particles of the active material carry the mechanical load. This time-dependent deformation requires porosity and continuously lowers the mechanical effect of the binder with time under load. This reduces the apparent thermal activation of E1 and η in the model. In essence, the conceptually simple Zener_k model cannot account for changes in the electrode structure during loading. Our interpretation of the reduced thermal activation of the electrode compared to pure PVDF is supported by the observation that the resistance of an electrode under cyclic load is not directly proportional to the electrode thickness when considering more than one cycle [6]. This observation implies that the particles in the electrode change their position which is also suggested to happen here during constant load where the binder may move from highly stressed regions between hard particles into the pore space. It may be assumed, that similar mechanisms are present in all composite electrodes that rely on viscous polymeric binders, such as PVDF.

4.4 | The Effects of a Solvent on the Mechanics of Binder and Electrode

Figure 10a shows stress jumps on pure PVDF polymer. The presence of the PC solvent reduces its stiffness and enhances the viscosity. Cyclic load tests on pure PVDF (black and blue curves in Figure 10b) show that the compressibility increases by a factor of about three after soaking the polymer in the PC solvent. This is in line with the literature where solvent-soaked PVDF binder has been reported to have a lower elastic modulus [23, 24]. For composite electrodes, we observe an increase in compressibility by soaking of a up to seven times (Figure 9). The discrepancy in the gain in compressibility by soaking with electrolyte between pure PVDF (3x) and the composite (7x) indicates that the greater deformability may not solely be due to the altered mechanics of the PVDF binder. This might be explained by additional rearrangement pathways that are enabled in the electrode. These may consist in the reorientation of particles and the associated stress relaxation. The compaction of a porous electrode due to

the reorientation of nonspherical particles under mechanical load was investigated by Becker et al. [25] using simulations. We suggest that the weakened binder joints allow for a higher degree of particle reorientation and therefore larger deformation of the electrode. The increased reorientation of particles is probably enabled by the lower modulus of the PVDF polymer but also supported by a reduced adhesive strength. According to the literature, PVDF immersed in solvents has a significantly lower adhesive strength [26] and shows reduced yield stress [27] and a lower elastic modulus [28]. In this way, the weakened binder enables enhanced particle motion leading to the observed higher compressibility of the electrode.

The rate sensitivity of the electrode is strongly affected by the solvent. Compared to the dry state, the solvent-soaked composite electrode shows a significantly stronger dependence of the displacement amplitude and hysteresis area on the applied stress rate (cf. Figure 9a,b). In Figure 9b the difference in displacement amplitude between the highest and the lowest rate is about 70%. This can be clearly linked to the binder material, as similar changes can be observed after the addition of the PC solvent to bulk PVDF (Figure S5c).

The uptake of solvent by the PVDF binder depends on the temperature, as reported by Liu et al. [13]. In experiments at 80°C, they observed a strong increase in the swelling ratio and a shorter time until a saturation of the solvent was reached. Our results show the consequences of the thermally increased solvent uptake on the mechanical response, which is displayed in Figure 10b. A temperature rise of ∼30 K leads to an increase in compressibility of about one third. An increased compliance of about 50% is also found in the dry material in Figure 10b. The addition of solvent at a given temperature increases the compressibility by about 200%. Both, the addition of a solvent or an increase in temperature alter the properties of the binder polymer in similar ways. The polymer becomes more elastically compliant and viscous, leading to enhanced hysteretic deformation. For PVDF, the presence of the solvent has a much stronger mechanical effect than a typical temperature change of 30 K that could happen during the operation of a battery.

The solvent changes the material properties of the binder polymer toward lower stiffness and lower viscosity. This effect can be enhanced by a temperature increase. The changes of the binder mechanics become apparent at the level of the electrode as can be seen in Figure 9, where the qualitative behavior, i.e., the shape of the curve, persists but the amount of deformation and the rate sensitivity changes between Figure 9a,b. We expect that the changes in the binder have a strong impact on the dynamics of the structure of the electrode during battery operation. The known general trends in the evolution of the electrode composite [6] will persist but the amount of electrode deformation increases similar to choosing a binder with lower glass transition temperature. This means that the adaption processes (settling) of an electrode during operation as described before [6] will be much more pronounced. Thickness changes of the electrode are enhanced and the rate sensitivity of thickness and resistivity of the electrode are increased compared to dry electrodes.

5 | Summary

The uptake and release of lithium ions by the active material in the composite electrode during battery operation causes mechanical stresses that act on all electrode particles including the conductive additive and the binder polymer. In this experimental work, we mimic battery operation by applying cyclic compressive mechanical stresses to electrode sheets and investigate their effect on the resistivity and the strain of composite electrodes. In a previous study [6], we reported on the general mechanical and electrical behavior of dry composite electrodes and their structural evolution during cycling. In the present work we address the effect of temperature and investigate in more detail how the binder polymer affects the mechanics of the composite electrode. Further we report on the effect of a liquid electrolyte which we simulate by adding a carbonate solvent to the electrode in our mechanical experiment.

The electronic resistance of composite electrodes is comprised of the bulk resistance of the composite and the resistance of the interface between the electrode and the current collector. For the LFP-based electrodes as used here, the interface resistance strongly dominates the resistance of the electrode. Increased compressive stress reduces both the electronic resistance of the interface and that of the bulk of the electrode. Despite a large difference in magnitude, our results indicate that the scaling with the applied stress is qualitatively similar for both resistance contributions. To elucidate the role of the binder for the mechanics of composite electrodes, we mechanically investigate pure PVDF and compare it with similar experiments on composite electrodes that contain PVDF. Stress–displacement curves of binder and composite electrodes are similar. For both samples, increasing temperatures lead to reduced moduli and decreased viscosities. Data were recorded for different temperatures and a Zener model was used to determine the (apparent) activation energies of the electrode and the pure binder material. The results show that the elastic short-term response of the composite electrode and the pure binder material agree and that a difference exists in the viscous behavior. We attribute the difference to the motion of the binder polymer inside the electrode away from highly stressed regions into pores. Based on this mechanism, we suggest that the binder polymer in combination with its neighboring pores is responsible for the largest part of the time-dependent deformation of a composite electrode. Temperature changes during battery operation lead to thickness changes of the electrodes caused by the reorientation of electrode particles including the motion of binder which are enhanced at higher temperatures.

The addition of a solvent to the electrode or to the pure binder leads to a strong loss in stiffness and decreases the viscosity. The soaked electrode and the soaked binder polymer behave similarly, again indicating that the binder material is mainly responsible for the irreversible and time-dependent mechanical and electrical behavior of composite electrodes. The choice of binder clearly affects the viscous behavior of an electrode. To provide a comparison for the commonly used PVDF, which has a low glass transition temperature, we also performed experiments with PAA; PAA has a higher glass transition temperature, which is responsible for the more reversible elastic behavior at RT. Cyclic experiments with different rates and up to 10^6 cycles show that irreversible thickness changes are rate dependent for PVDF while for PAA they are rate-independent and scale with the time of load application.

The data presented here highlight the strong effect of the binder for the evolution of the structure of composite electrodes during battery operation. Both, increased temperature and the presence of carbonate solvents change the PVDF polymer and make

electrodes more elastically compliant and viscous, i.e., rate dependent. The addition of the electrolyte solvent, which is essential for an operational battery, has a very profound effect: It amplifies the impact of stress rate and temperature on the structural evolution. Thickness changes of dry electrodes were already detected after individual mechanical cycles with cycle times below 1 min [6]. With the observed enhanced mobility of the electrode enabled by the electrolyte and temperature, the response time of the electrode structure will be even faster. Therefore, the observed effects are expected to be ubiquitous in batteries and cause particle rearrangements in composite electrodes under all application conditions. This impacts the resistivity and thus can affect the performance and reliability of composite electrodes in operation.

Acknowledgments

The authors want to thank Dorit Nötzel and Ravika Goyal for preparing the electrode sheets. This work contributes to the research performed at CELEST (Center for Electrochemical Energy Storage Ulm-Karlsruhe). T. B. gratefully acknowledges the funding and support by the German Research Foundation (DFG) within the research training group SiMET under the project number 281041241/GRK2218.

Open Access funding enabled and organized by Projekt DEAL.

Funding

This work was supported by the Deutsche Forschungsgemeinschaft (281041241).

Conflicts of Interest

The authors declare no conflicts of interest.

Data Availability Statement

The data that support the findings of this study are available from the corresponding author upon reasonable request.

References

1. C. R. Birkl, M. R. Roberts, E. McTurk, P. G. Bruce, and D. A. Howey, "Degradation Diagnostics for Lithium Ion Cells," *Journal of Power Sources* 341 (2017): 373–386.

2. F. Pistorio, D. Clerici, F. Mocera, and A. Somà, "Review on the Experimental Characterization of Fracture in Active Material for Lithium-Ion Batteries," *Energies* 15 (2022): 9168.

3. H. C. W. Parks, A. M. Boyce, A. Wade, et al., "Direct Observations of Electrochemically Induced Intergranular Cracking in Polycrystalline NMC811 Particles," *Journal of Materials Chemistry A* 11 (2023): 21322–21332.

4. D. Chen, D. Kramer, and R. Mönig, "Chemomechanical Fatigue of $LiMn_{1.95}Al_{0.05}O_4$ Electrodes for Lithium-Ion Batteries," *Electrochimica Acta* 259 (2018): 939–948.

5. A. Mukhopadhyay and B. W. Sheldon, "Deformation and Stress in Electrode Materials for Li-Ion Batteries," *Progress in Materials Science* 63 (2014): 58–116.

6. T. Brendel, M. Janzen, M. Müller, W. Bauer, D. Kramer, and R. Mönig, "The Dynamics of the Structure of Composite Electrodes during Their Operation in Lithium-Ion Batteries," *Energy Technology* 13 (2025): 2500106.

7. M. Janzen, *Mechanical Investigations of Composite Electrodes for Li-Ion Batteries, Thesis*, (Karlsruhe University of Technology, 2025).

8. J. Entwistle, R. Ge, K. Pardikar, R. Smith, and D. Cumming, "Carbon Binder Domain Networks and Electrical Conductivity in Lithium-Ion Battery Electrodes: A Critical Review," *Renewable and Sustainable Energy Reviews* 166 (2022): 112624.

9. Z. Choi, D. Kramer, and R. Mönig, "Correlation of Stress and Structural Evolution in $Li_4Ti_5O_{12}$-Based Electrodes for Lithium Ion Batteries," *Journal of Power Sources* 240 (2013): 245–251.

10. S. P. V. Nadimpalli, V. A. Sethuraman, D. P. Abraham, A. F. Bower, and P. R. Guduru, "Stress Evolution in Lithium-Ion Composite Electrodes during Electrochemical Cycling and Resulting Internal Pressures on the Cell Casing," *Journal of the Electrochemical Society* 162 (2015): A2656–2663.

11. A. Chanda, A. Pakhare, A. Alfadhli, V. A. Sethuraman, and S. P. V. Nadimpalli, "Real-Time Measurement of Sodiation Induced Stress in Hard Carbon Composite Electrodes," *Journal of Power Sources* 609 (2024): 234678.

12. HIOKI EE CORPORATION, "*RM2610 Electrode Resistance Measurement System Instruction Manual*," Can Be Found under 2025 (accessed, 26 May 2025), https://www.hioki.com/Euro-en/products/Resistance-Meters/Resistance/id_6740.

13. W.-R. Liu, M.-H. Yang, H.-C. Wu, S. M. Chiao, and N.-L. Wu, "Enhanced Cycle Life of Si Anode for Li-Ion Batteries by Using Modified Elastomeric Binder," *Electrochemical and Solid-State Letters* 8 (2005): 100.

14. A. R. Greenberg and R. P. Kusy, "Viscoelastic Behavior of Highly Crosslinked Poly(acrylic Acid)," *Journal of Applied Polymer Science* 25 (1980): 2795–2805.

15. X.-D. Fan, Y.-L. Hsieh, J. M. Krochta, and M. J. Kurth, "Study on Molecular Interaction Behavior, and Thermal and Mechanical Properties of Polyacrylic Acid and Lactose Blends," *Journal of Applied Polymer Science* 82 (2001): 1921–1927.

16. A. Linares and J. L. Acosta, "Tensile and Dynamic Mechanical Behaviour of Polymer Blends Based on PVDF," *European Polymer Journal* 33 (1997): 467–473.

17. A. D. Mulliken and M. C. Boyce, "Mechanics of the Rate-Dependent Elastic–plastic Deformation of Glassy Polymers from Low to High Strain Rates," *International Journal of Solids and Structures* 43 (2006): 1331–1356.

18. A. Zosel, "Adhesion and Tack of Polymers: Influence of Mechanical Properties and Surface Tensions," *Colloid & Polymer Science* 263 (1985): 541–553.

19. E. N. Primo, M. Chouchane, M. Touzin, P. Vazquez, and A. A. Franco, "Understanding the Calendering Processability of $Li(Ni_{0.33}Mn_{0.33}Co_{0.33})O_2$-Based Cathodes," *Journal of Power Sources* 488 (2021): 229361.

20. J. S. Terreblanche, D. L. Thompson, I. M. Aldous, J. Hartley, A. P. Abbott, and K. S. Ryder, "Experimental Visualization of Commercial Lithium Ion Battery Cathodes: Distinguishing Between the Microstructure Components Using Atomic Force Microscopy," *Journal of Physical Chemistry C* 124 (2020): 14622–14631.

21. V. Vanpeene, L. Huet, J. Villanova, et al., "Deciphering the Benefits of Coordinated Binders in Si-Based Anodes by Combined Operando/In Situ and Ex Situ X-Ray Micro- and Nano-Tomographies," *Advanced Energy Materials* 15 (2025): 2403741.

22. E. W. Andrews, L. J. Gibson, and M. F. Ashby, "The Creep of Cellular Solids," *Acta Materialia* 47 (1999): 2853–2863.

23. A. Magasinski, B. Zdyrko, I. Kovalenko, et al., "Toward Efficient Binders for Li-Ion Battery Si-Based Anodes: Polyacrylic Acid," *ACS Applied Materials & Interfaces* 2 (2010): 3004–3010.

24. Q. D. Nguyen, E.-S. Oh, and K.-H. Chung, "Nanomechanical Properties of Polymer Binders for Li-Ion Batteries Probed with Colloidal Probe Atomic Force Microscopy," *Polymer Testing* 76 (2019): 245–253.

25. V. Becker, O. Birkholz, Y. Gan, and M. Kamlah, "Modeling the Influence of Particle Shape on Mechanical Compression and Effective Transport Properties in Granular Lithium-Ion Battery Electrodes," *Energy Technology* 9 (2021): 2000886.

26. S. Komaba, K. Shimomura, N. Yabuuchi, T. Ozeki, H. Yui, and K. Konno, "Study on Polymer Binders for High-Capacity SiO Negative Electrode of Li-Ion Batteries," *Journal of Physical Chemistry C* 115 (2011): 13487–13495.

27. M. R. Janvrin and A. M. Grillet, "Strain and Conductivity in Lithium Ion Battery Binders," (U.S. Department of Energy, Office of Scientific and Technical Information, 2019), https://doi.org/10.2172/1561807.

28. A. M. Grillet, T. Humplik, E. K. Stirrup, et al., "Conductivity Degradation of Polyvinylidene Fluoride Composite Binder during Cycling: Measurements and Simulations for Lithium-Ion Batteries," *Journal of the Electrochemical Society* 163 (2016): 1859–1871.

Supporting Information

Additional supporting information can be found online in the Supporting Information section.